Solvent coarsening around colloids driven by temperature gradients

Sutapa Roy,[1,2] Siegfried Dietrich,[1,2] and Anna Maciolek[3]

[1]*Max-Planck-Institut für Intelligente Systeme, Heisenbergstrasse 3, 70569 Stuttgart, Germany*
[2]*IV. Institut für Theoretische Physik, Universität Stuttgart, Pfaffenwaldring 57, 70569 Stuttgart, Germany*
[3]*Institute of Physical Chemistry, Polish Academy of Sciences, Kasprzaka 44/52, PL-01-224 Warsaw, Poland*

Using mesoscopic numerical simulations and analytical theory, we investigate the coarsening of the solvent structure around a colloidal particle emerging after a temperature quench of the colloid surface. Qualitative differences in the coarsening mechanisms are found, depending on the composition of the binary liquid mixture forming the solvent and on the adsorption preferences of the colloid. For an adsorptionwise neutral colloid, the phase next to its surface alternates as a function of time. This behavior sets in on the scale of the relaxation time of the solvent and is absent for colloids with strong adsorption preferences. A Janus colloid, with a small temperature difference between its two hemispheres, reveals an asymmetric structure formation and surface enrichment around it, even if the solvent is within its one-phase region and if the temperature of the colloid is above the critical demixing temperature T_c of the solvent. Our phenomenological model turns out to capture recent experimental findings according to which, upon laser illumination of a Janus colloid and due to the ensuing temperature gradient between its two hemispheres, the surrounding binary liquid mixture develops a concentration gradient.

I. INTRODUCTION

Coarsening is a paradigmatic example for nonequilibrium dynamics of systems approaching a steady state. Typically, this process is induced by a temperature quench of an initially homogeneous two-phase system, such as a binary liquid mixture or a polymer mixture, into the regime of immiscibility. The dynamics of coarsening, which has been studied intensively for bulk fluid [1,2], is changed substantially by the presence of surfaces. In this latter context, a lot of attention has been paid to binary fluids in contact with planar surfaces in semi-infinite or film geometries. Strong efforts have been devoted to phase separation guided by the surface, which occurs if – as is generically the case – the surface prefers one species of the binary fluid over the other. Under such conditions, upon a temperature quench of an initially homogeneous system into the miscibility gap, plane composition waves propagate from the surface into the bulk and result in a transient layer structure [3]. There are numerous studies of this so-called surface-directed phase-separation process [4,5]. Most of them assume that after a quench the system – including its boundaries – thermalizes instantaneously so that the coarsening proceeds at constant temperature everywhere. Instead of quenching, one can apply temperature gradients, e.g., by heating or cooling the boundary of a system. There is much less theoretical work concerning phase separation induced by temperature gradients, in spite of such conditions being created in various experiments and for practical applications, e.g., in polymer systems [6–10]. So far, the focus has been on systems bounded by "planar" and "neutral" surfaces (i.e., with no preference for either component of a two-phase system), supplemented by boundary conditions that maintain a *stationary* linear temperature gradient across a film [8,9,11,12]. The effects associated with a temperature quench of a boundary, whereupon the temperature gradient across the

system varies in time, has rarely [13,14] been considered, albeit for a planar geometry. To the best of our knowledge, in this context the effects due to spatiotemporal temperature gradients in fluids bounded by non-neutral surfaces, i.e., in the generic presence of surface fields, have not yet been explored.

Here we consider a spherical colloid suspended in a near-critical binary solvent, kept in its mixed phase above T_c. We study the dynamics of solvent coarsening following a temperature quench of the surface of the suitably coated colloid. Our interest in this problem has been triggered by recent experiments with a partially gold-capped Janus colloid suspended in a mixed phase of water-lutidine mixture below its lower critical point [15,16], in which, upon laser illumination with sufficient intensity, one observes phase separation of the solvent around the particle. The *early* stage dynamics of this complex process has not yet been investigated. A steady state occurring at *late* times has been considered in the studies of moving Janus colloids for quenches crossing the binodal [17,18]. In these studies, the assumption has been made that the order parameter starts to evolve only after the stationary temperature profile has been reached. Here, we consider the *simultaneous* time evolution of the coupled order parameter and temperature fields. This is expected to have repercussions for the motion of the Janus colloids.[1] For homogeneous colloids, we observe a surprising pattern evolution, which cannot

————

[1]Allowing for the simultaneous evolution of coupled temperature and OP fields revealed that the body force exerted on a colloid due to the concentration flux is much stronger at the beginning of the coarsening process than in the stationary state. This suggests that the motion of the Janus particle may start before the stationary state is achieved.

be captured by the above assumption. For Janus particles we show that, unexpectedly, also temperature quenches, which *do not* cross the binodal, lead to structure formation. Our work addresses coarsening phenomena in the presence of a time-dependent temperature gradient and symmetry-breaking surface field, which, to the best of our knowledge, have not yet been studied, as was mentioned before.

II. MODEL AND METHOD

We employ a phenomenological model, which we treat numerically and analytically. Specifically, we use the Cahn-Hilliard-Cook (CHC) -type description, based on the Landau-Ginzburg free-energy functional conjoined with the heat diffusion equation [1,13]:

$$\frac{\partial \psi(\mathbf{r},t)}{\partial t} = \nabla^2 \left(\frac{\tilde{T}(\mathbf{r},t)}{|\tilde{T}_1|} \psi(\mathbf{r},t) + \psi^3(\mathbf{r},t) - \nabla^2 \psi(\mathbf{r},t) \right) + \eta(\mathbf{r},t), \tag{1a}$$

$$\frac{\partial \tilde{T}(\mathbf{r},t)}{\partial t} = \mathcal{D} \nabla^2 \tilde{T}(\mathbf{r},t). \tag{1b}$$

Here $\psi(\mathbf{r},t)$ is the local order parameter (OP) and $\tilde{T}(\mathbf{r},t)$ is proportional to the reduced temperature field $(T(\mathbf{r},t) - T_c)/T_c$. T_1 is the quench temperature of the colloid surface. Note that the coupling between the temperature and OP fields is captured by the first term on the right-hand side of Eq. (1a). The Gaussian random noise obeys the relation $\langle \eta(\mathbf{r},t)\eta(\mathbf{r}',t') \rangle = -2\nu(\mathbf{r})\nabla^2 \delta(\mathbf{r} - \mathbf{r}')\delta(t - t')$; $\nu(\mathbf{r})$ is the strength of noise. Equation (1) is valid for phase separation driven by diffusion, with hydrodynamic effects being irrelevant (e.g., for small Péclet numbers or at the early time of coarsening). $\mathcal{D} = D_{th}/(|\tilde{T}_1| D_m)$ involves the ratio of the thermal diffusivity D_{th} of the solvent and the solvent interdiffusion constant D_m. Equation (1) has to be complemented by boundary conditions (BCs) on the surface $\mathscr{S}$ of the colloid. At a homogeneous surface, the temperature field is constant, $\tilde{T}(\mathbf{r})|_{\mathscr{S}} = \tilde{T}_1$, and we assume there is no heat flux through the colloid. The generic preference of the colloid surface for one of the two components of the binary mixture is accounted for by the so-called Robin BC $[\hat{n} \cdot \nabla \psi(\mathbf{r}) + \alpha \psi(\mathbf{r})]|_{\mathscr{S}} = h_s$ [19]. Here, α and h_s are the dimensionless surface enhancement parameter and symmetry-breaking surface field, respectively. The second necessary BC [20] is for no particle flux normal to the surface. Figure 1 explains various notations. The spherical colloid of radius R is placed at the center of a cubic simulation box (SB) with side length L and periodic boundary conditions [21] at the side walls of the SB. (For details concerning the model and numerical techniques, see Appendix A. Relationships to experimentally relevant quantities are given in Appendix B.)

III. RESULTS

We first study demixing near a homogeneous colloid ($h_s = $ const and $\tilde{T}_l = \tilde{T}_r = -1$) quenched from $\tilde{T}_i = 1$ to -1, with a spatially averaged off-critical solvent concentration $\psi_0 = 0.1$. Figure 2(a) portrays a typical temperature profile in the midplane $z = L/2$ of the simulation box at an early time $t = 10$. There is a strong temperature gradient, with $\tilde{T}(\mathbf{r})$ near the side walls of the simulation box being close to the initial value $\tilde{T}_i = 1$. As demonstrated in Fig. 3, this temperature gradient
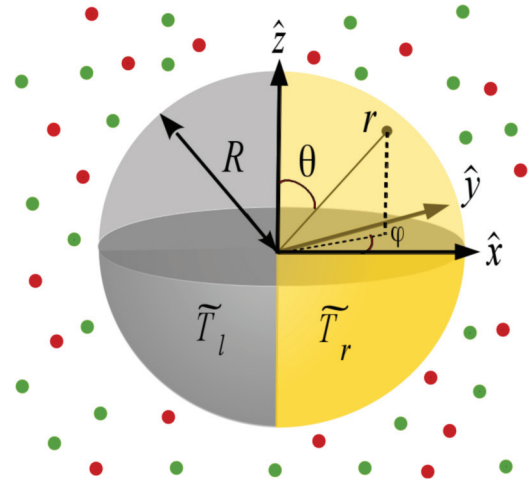
FIG. 1. Spherical Janus colloid of radius R with reduced temperatures $\tilde{T}_r$ and $\tilde{T}_l$ on its right and left hemisphere, respectively. The azimuthal angle φ is measured from the x axis in the horizontal $\hat{x} \hat{y}$ midplane of the colloid, the polar angle θ is measured from the z axis, and r is the radial distance from the center. The initial temperature in the whole binary solvent is $\tilde{T}_i = \tilde{T}_r$.

reduces with time and the angularly averaged concentration profile attains sinusoidal shape due to surface layer formation (see Fig. 4). As noted before, the dynamics of coarsening was studied extensively for instantaneous quenches [22], but never for a time-dependent temperature gradient with symmetry-breaking surface fields.

In Fig. 2(b), we show a cross-sectional ($\hat{x} \hat{y}$) view of the evolution patterns at six times. As the solvent cools, a layered structure, consisting of disconnected concentric circular shells, forms near the colloid. Two neighboring layers contain opposite phases, while the phase next to the colloid is $\psi > \psi_0$. Away from the colloid, spinodal-like patterns prevail (see $t = 100$). Upon increasing time, the shell structure propagates into bulk via the formation of new layers, and the maximal absolute value of the angularly averaged concentration in each layer increases (see the radial concentration profiles in Fig. 4, which evolved from a randomly chosen initial configuration). At early times, demixing at the surface is dominant, while in the bulk the order parameter retains its initial value.

Since a reliable analytic expression for OP in the presence of temperature gradients could not yet be obtained, numerical results are indispensable. In Fig. 2(c), we present numerical results (■) for $\psi(r,t)$ after quenching a homogeneous colloid (not the solvent) to below T_c, i.e., with temperature gradient. The dashed line refers to our solution for a linearized approximation of Eq. (1) without noise and temperature gradient, with the approximate form (by including h_s in the calculations in [13,23])

$$\psi(\zeta = r - R, t) \approx \psi_0 + \left[(-\alpha \psi_0 + h_s)/(k_f^3 \sqrt{\pi t}) \right]$$
$$\times [R/(R + \zeta)] \exp \left[k_f^4 t - \zeta^2/(16 k_f^2 t) \right]$$
$$\times \left\{ A \cos k_f \zeta - [\zeta/(4 k_f^3 t)] \sin k_f \zeta \right\}, \tag{2}$$

where $A = 1 + [5/(8 k_f^4 t)][1 - \zeta^2/(8 k_f^2 t)]$, with $k_f^2 = (1 - 3\psi_0^2)/2$ characterizing the fastest growing mode. In
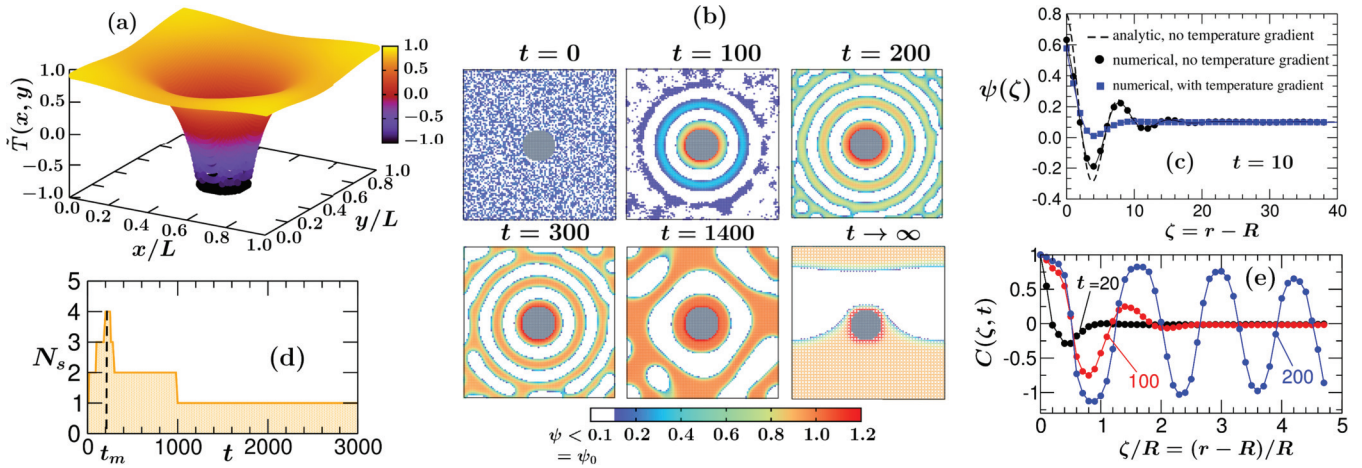
FIG. 2. Temperature-gradient induced demixing around a homogeneous colloid immersed in a binary solvent with off-critical concentration $\psi_0 = 0.1$ and undergoing slow cooling below T_c. The results in (a), (b), (d), and (e) correspond to $L = 100$, $R = 10$, $\alpha = 0.5$, $h_s = 1$, $\mathcal{D} = 50$, and $\nu = 10^{-4}$. (a) Temperature profile in the midplane $z = L/2$ at an early time $t = 10$, exhibiting a strong gradient. Initially, the solvent is hot and the colloid is cold. (b) Coarsening patterns in the midplane of the colloid. Close to the colloid, disconnected concentric circular structures form; away from the colloid, spinodal-like patterns prevail. As time progresses, the shells propagate into bulk via the formation of new layers. As expected, in the long-time limit the system forms a planar interface trapping the colloid. (c) Comparison of the approximate analytic prediction of the OP profile without any temperature gradient ($\bullet$) and numerical data ($\blacksquare$) with a temperature gradient, for $R = 10$, $\tilde{T}_i = 1$, $\alpha = 0.01$, $h_s = 0.1$, and $\nu = 10^{-4}$. (d) Nonmonotonic time dependence of the number of concentric shells N_s; the decrease is much slower than the increase. (e) Radial two-point equal-time correlation function $C(\zeta = r - R, t)$ vs reduced distance ζ/R for three values of t. $C(\zeta, t)$ decays spatially fast at early times, while with increasing time it develops multiple minima corresponding to concentric shell-like layers around the colloid. Data have been averaged over 10 independent initial configurations.

Fig. 2(c), we also present numerical data for the colloid (homogeneous) and the solvent being quenched together to $\tilde{T} = -1$, i.e., in the absence of temperature gradients. The slight discrepancy between the numerical data for this case and the corresponding analytic prediction is likely to be due to the linear approximation used for the theory. Numerical data with a temperature gradient ($\blacksquare$) exhibit smaller peaks compared to the overall quench. The reason is that in the case of a gradient, temperature fronts propagate from the colloid into the bulk slowly, and thus coarsening proceeds slowly. Thereby, at $t = 10$, while the OP profile for an instantaneous overall quench has already developed two prominent minima, for cooling it has acquired only one minimum, the absolute value of which is also smaller.

Figure 3 depicts the temperature profiles at $t = 10$ and 200. In the course of time, the temperature gradient decreases due to cooling, the temperature front moves away from the surface, and the fluid ahead generates new layers. Once the layered patterns have spread throughout the finite-sized system, a new phenomenon occurs: the layers start to break up due to bulk spinodal decomposition, and the number of shells decreases [see the case $t = 1400$ in Fig. 2(b)].

Exemplary results concerning the nonmonotonic behavior of the number of concentric shells $N_s(t)$ in Fig. 2(d) indicate a novel coarsening mechanism, likely due to an interplay of
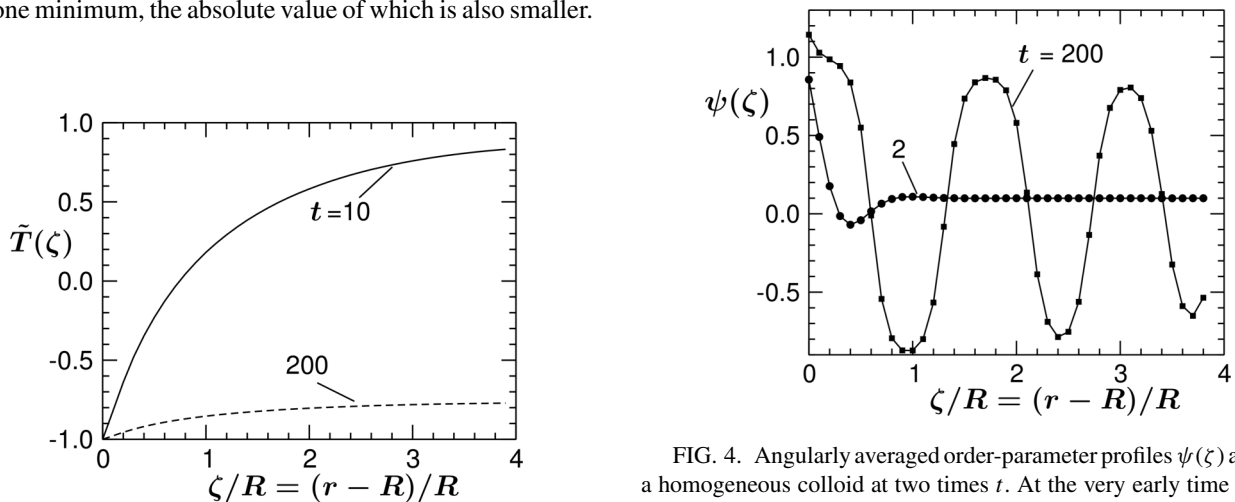
FIG. 3. Angularly averaged temperature profile $\tilde{T}(\zeta)$ around a homogeneous colloid. The temperature gradient decreases with time. The results correspond to the same parameters as used in Fig. 4.

FIG. 4. Angularly averaged order-parameter profiles $\psi(\zeta)$ around a homogeneous colloid at two times t. At the very early time $t = 2$, surface demixing prevails while in the bulk $\psi(\zeta)$ attains its initial value $\psi_0 = 0.1$. Over the course of time, new layers form and the maximum value of $\psi(\zeta)$ increases. The lines interpolate the data points. The parameter values are those used in Fig. 3.
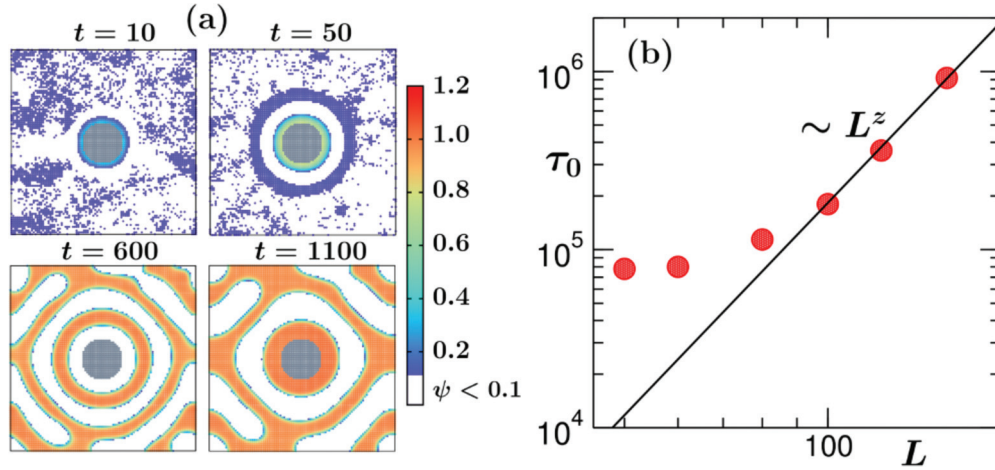
FIG. 5. (a) Snapshots of a cooling binary solvent ($\psi_0 = 0.1$) around an adsorption-neutral, homogeneous colloid. At early times, the phase $\psi > \psi_0$ is formed near the colloid surface until at $t \simeq 600$ the phase near the surface is replaced by the one with $\psi < \psi_0$. Results correspond to $L = 100$, $R = 10$, $\tilde{T}_1 = -1 = \tilde{T}_l = \tilde{T}_r$, $\alpha = 0$, $h_s = 0$, and $\nu = 10^{-4}$. (b) Plot of the crossover time τ_0 vs system size L for $R = 5$. The solid line drawn through the rightmost data points refers to the finite-size critical relaxation time $\propto L^z$; $z = 4$ (see the main text).

surface and bulk demixing. The growth and the decay of $N_s(t)$ are not symmetric about the time t_m at which N_s peaks; the breakup is much slower.

In order to investigate the surface patterns around the colloid, we compute the radial two-point equal-time correlation function in the midplane defined as $C(\zeta = r - R, t) = \langle \psi(R,t)\psi(R + \zeta,t) \rangle - \langle \psi(R,t) \rangle \langle \psi(R + \zeta,t) \rangle$. The symbol $\langle \cdot \rangle$ denotes the average over initial configurations of the angularly averaged $C(\zeta, t)$. For self-similar domains in bulk, $C(r,t)$ exhibits scaling [22]: $C_{\text{bulk}}(r,t) = \mathscr{C}(r/\ell(t))$, where $\mathscr{C}$ is for bulk and static equilibrium. $\ell(t)$ is the mean domain size. In Fig. 2(e), $C(\zeta,t)$ is plotted versus distance ζ/R for three t. While at early times $C(\zeta,t)$ decays spatially faster, upon increasing time the spatial decay becomes less steep and $C(\zeta,t)$ develops multiple peaks corresponding to various surface layers. However, we could not find any data collapse for $C(r,t)$ onto a function of a single variable. This indicates *non*-self-similarity of coarsening patterns due to symmetry-breaking surface fields.

We have explored also the coarsening process around an adsorption-neutral colloid ($\alpha = 0, h_s = 0$). For an off-critical solvent, the qualitative feature of the coarsening patterns for a neutral colloid [Fig. 5(a)] is similar to that with surface adsorption preferences [Fig. 2(b)]. However, there is an important difference concerning the phase formed at the colloid surface. While for $h_s > 0$ the phase with $\psi > \psi_0$ remains at the surface at all times, for the neutral colloid a crossover occurs: at very early times the phase $\psi > \psi_0$ is dominant near the surface until the layered structures have spread throughout the system. Thereafter, beyond a certain crossover time τ_0 [see the panel for $t = 600$ in Fig. 5(a)] the phase $\psi < \psi_0 = 0.1$ is formed near the surface. We anticipate this first crossover time τ_0 to be proportional to the OP relaxation time τ [24] of the solvent. For a near-critical system $\tau \propto \xi^z$, where ξ is the equilibrium bulk correlation length. Thus for a finite system at $T_{c,\text{bulk}}$ it scales as $\tau \propto L^z$ [25]; $z \simeq 4$ is the dynamic critical exponent for model B [25] with diffusive dynamics for the conserved order parameter [Eq. (1a)]. In Fig. 5(b), data for τ_0 are plotted for various system sizes. Agreement

with the aforementioned power-law behavior (solid line) on a double-logarithmic scale supports the expectation $\tau_0 \sim \tau$. Such a crossover is observed only for adsorption-neutral colloids, off-critical concentrations, and the simultaneous time evolution of coupled OP and temperature fields. For the time evolution of the OP with stationary temperature profiles or for a critical concentration, both phases always form near the surface, and the OP morphology is not shell-like but wormlike.

Next, we turn to coarsening of the solvent around a *Janus* colloid with two hemispheres at different temperatures; both hemispheres prefer the same component of the solvent but with different strengths. Figure 6(a) shows OP distributions. We start with a homogeneous configuration of the binary solvent at $\tilde{T} = 1$ and keep both hemispheres of the Janus colloid at $\tilde{T} = 1$ (above T_c) at $t = 0$. Subsequently, we let the system evolve ($t = 1 - 400$) such that there is no temperature gradient. Accordingly, the surface enrichment phenomenon is the only mechanism for structure formation. The snapshot at $t = 400$ corresponds to the equilibrium surface adsorption OP profile. The Janus character of the colloid causes only weak deviations from a spherically symmetric adsorption profile. Next, at $t = 401$ we quench the left hemisphere of the Janus colloid to $\tilde{T} = 0.7$ such that the subsequent evolution will occur in the presence of a temperature gradient. The corresponding stationary configuration is shown at $t = 1400$. A comparison of the snapshots at $t = 400$ and 1400 clearly demonstrates the difference between the equilibrium surface pattern formed due to surface enrichment only and the steady-state pattern emerging in the presence of a temperature gradient. Clearly, a temperature gradient leads to a more pronounced bubble formation on the cold side of the Janus colloid. Coarsening in fluid regions with $T > T_c$ was observed experimentally [6] in polymer solutions due to the Soret effect and numerically [14] in fluid mixtures due to convective flows. Here, for *purely diffusive* dynamics, i.e., without involving any hydrodynamic flow, we observe the condensation of a droplet around the colloid above T_c, which is a novel phenomenon due to the combination of Soret and surface effects. Although this is
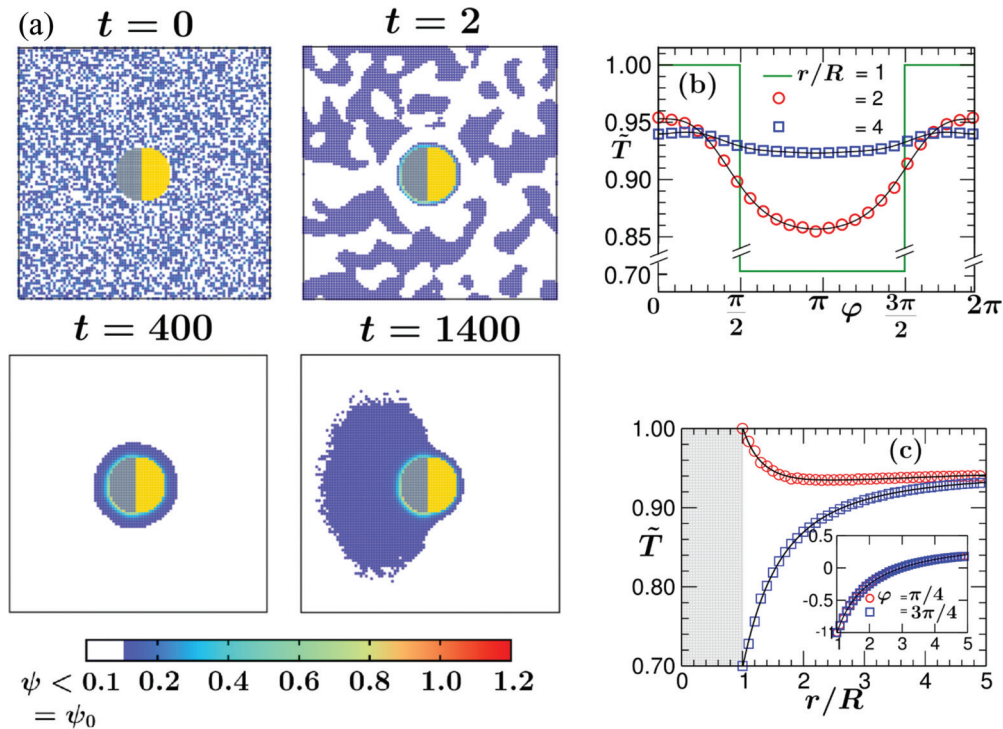
FIG. 6. Coarsening of a binary solvent with $\psi_0 = 0.1$ around a Janus colloid. Results correspond to $L = 100$, $R = 10$, $\alpha = 0.5$, $h_{s,l} = 1$, $h_{s,r} = 0.5$, and $\nu = 10^{-5}$. (a) Evolution patterns in its midplane ($\theta = \pi/2$). The left and right hemispheres are gray and yellow, respectively. Initially, both the solvent and colloid are at $\tilde{T} = 1$. From $t = 1$ to 400, the system evolves at constant temperature everywhere. At $t = 401$, the temperature of the left hemisphere is quenched to $\tilde{T}_l = 0.7$. The corresponding stationary configuration is shown at $t = 1400$. Although both hemispheres are maintained above T_c, structure formation is observed. (b) Temperature distribution $\tilde{T}(r,\varphi) > 0$ of the solvent in the midplane around a Janus colloid. Dependence (b) on the azimuthal angle φ for two radial distances r from the colloid center and (c) on r for two opposite angles φ corresponding to the right and to the left hemisphere, respectively. The shaded region in (c) corresponds to the space occupied by the colloid. Inset of (c): as in the main figure, but for the homogeneous colloid discussed in Fig. 2 for which there is no dependence on φ.

reminiscent of so-called surface enrichment, the mechanism, as explained above, is very different.

To relate the anisotropy of surface patterns with temperature gradients, within the midplane we have computed the radial and angular dependence of $\tilde{T}$ on r and φ, respectively. Figure 6(b) depicts the dependence of $\tilde{T}$ on φ for two fixed values of r with temperature in a stationary state. The symbols correspond to our numerical data; the solid lines refer to analytical predictions [26]: $\tilde{T}(r,\varphi) = A_0 + \sum_{n=0}^{\infty} B_n P_n(\cos\varphi)(R/r)^{n+1}$, where B_n are constants and $\{P_n\}$ are Legendre polynomials. In Fig. 6(c) we plot the radial dependence of $\tilde{T}$ for two opposite angles. Our numerical results agree with the theoretical predictions. The very slow (algebraic) decay of the stationary temperature profile facilitates coarsening in extended regions of the system; in our simulation box, it takes place everywhere. Due to its finite size, away from the colloid $\tilde{T}$ is lower than its initial value. Note that $\tilde{T}(r,\varphi)$ is anisotropic, i.e., different for the two angles considered. This should be compared with the homogeneous colloid for which $\tilde{T}(r)$ is radially symmetric [see the inset of Fig. 6(c)] and coarsening patterns are also symmetric [Fig. 2(b)]. This confirms that the anisotropy of the temperature distribution is the dominant source of anisotropy in the OP distribution around a Janus colloid. Upon increasing the radius of the colloid, the radial extent of a stationary bubble of the phase preferred by the colloid and the amplitude of the OP profile increase moderately. The value of the OP at the

left hemisphere surface is slightly larger than at a planar wall ($R \to \infty$). At the right hemisphere it is reduced to about half the value for a planar wall.

IV. SUMMARY

In summary, we have studied the nonequilibrium phenomena of a temperature-gradient-induced coarsening and the formation of the concentration distribution around a heated colloid suspended in a binary solvent. Coarsening patterns depend on the adsorption preferences of the colloid surface and on the bulk concentration of the solvent. For deep quenches (corresponding to $\mathcal{D} \approx 100$), the timescale of patterns for a molecular solvent varies between 10^{-1} and 10^{-2} s, depending on the size of the colloid and the simulation box (see the Appendix B). There is an anisotropic structure formation around a Janus colloid even if the colloid and the solvent are at temperatures corresponding to its one-phase region, which is different from *surface enrichment* [4,27,28]. Even if $\tilde{T}(\mathbf{r},t)$ exhibits a fast dynamics, the results of our study are relevant for controlling pattern formation, e.g., in polymers, using hot homogeneous or Janus particles [29]. It is expected that the patterns due to the temperature gradient will be different from those seen for spatially homogeneous quenches. Expressing the dimensionless parameters used in our study in terms of dimensional quantities (see Appendix B) suggests that the behavior described above is experimentally accessible, e.g.,

for colloids of size $\simeq 20$ μm within 3–4 min. Our study contributes to the understanding of the propulsion mechanism via diffusive dynamics for one of the commonly used representatives of synthetic active matter [15,16] [see (1)]. The other presently available theoretical approaches [17,18] are based instead on hydrodynamics and are complementary to our study. Generally, dipping a particle into its binary solvent causes transportation of the preferred phase toward its surface. From our study, we conclude that this transport is strongly enhanced if supported by a time-dependent temperature gradient.

APPENDIX A: MODEL

Our starting point is a dynamical equation for the conserved OP that has the form of a continuity equation,

$$\frac{\partial \mathring{\psi}(\mathbf{r},t)}{\partial t} = -\boldsymbol{\nabla} \cdot \mathring{\boldsymbol{j}}(\mathbf{r},t), \tag{A1}$$

where the OP flux $\mathring{\boldsymbol{j}}$ is proportional to the gradient of the local chemical potential:

$$= -\boldsymbol{\nabla} \cdot [-M\boldsymbol{\nabla}\mu(\mathbf{r},t)] = M\nabla^2 \frac{\delta \mathcal{F}[\psi]}{\delta \psi(\mathbf{r},t)}; \tag{A2}$$

M is the mobility of the order parameter. Using for $\mathring{\mathcal{F}}$ the form of the Landau-Ginzburg free-energy functional $\frac{\mathcal{F}}{k_B T_c} = \int (d^d\mathring{r}/v)[\frac{1}{2}a\psi(\mathbf{r})^2 + \frac{1}{4}u\psi(\mathbf{r})^4 + \frac{1}{2}C(\nabla\psi(\mathbf{r}))^2]$, with $a \propto (T - T_c)/T_c$, one obtains the Cahn-Hilliard-Cook (CHC) equation

$$\frac{\partial \mathring{\psi}(\mathring{r},\mathring{t})}{\partial \mathring{t}} = (M/v)k_B T_c \mathring{\nabla}^2$$
$$\times [a\mathring{\psi}(\mathring{r},\mathring{t}) + u\mathring{\psi}^3(\mathring{r},\mathring{t}) - C\mathring{\nabla}^2\mathring{\psi}(\mathring{r},\mathring{t})], \tag{A3}$$

where v is a microscopic volume unit, such as the volume of a unit cell of a lattice or a molecular volume of the species forming a binary liquid mixture. For a spatially varying temperature field $\tilde{T}(\mathring{r}) = \mathcal{A}(T(\mathring{r}) - T_c)/T_c$, we replace the constant parameter a by $\tilde{T}(\mathbf{r},t)$ and consider the following stochastic equation:

$$\frac{\partial \mathring{\psi}(\mathring{r},\mathring{t})}{\partial \mathring{t}} = (M/v)k_B T_c \mathring{\nabla}^2[\tilde{T}(\mathring{r},\mathring{t})\mathring{\psi}(\mathring{r},\mathring{t})$$
$$+ u\mathring{\psi}^3(\mathring{r},\mathring{t}) - C\mathring{\nabla}^2\mathring{\psi}(\mathring{r},\mathring{t})] + \mathring{\eta}(\mathring{r},\mathring{t}). \tag{A4}$$

The Gaussian white noise η with zero mean value represents thermal fluctuations and satisfies the relation

$$\langle \mathring{\eta}(\mathring{r},\mathring{t})\mathring{\eta}(\mathring{r}',\mathring{t}')\rangle = -2(M/v)k_B T(\mathring{r})\mathring{\nabla}^2\delta(\mathring{r} - \mathring{r}')\delta(\mathring{t} - \mathring{t}'). \tag{A5}$$

Here we have assumed local equilibrium so that the noise obeys the fluctuation-dissipation theorem. We take the temperature field $\tilde{T}(\mathring{r},\mathring{t})$ to be a solution of the heat diffusion (HD) equation

$$\frac{\partial \tilde{T}(\mathring{r},\mathring{t})}{\partial \mathring{t}} = D_{\text{th}}\mathring{\nabla}^2\tilde{T}(\mathring{r},\mathring{t}), \tag{A6}$$

where D_{th} is the thermal diffusivity of the solvent with the boundary conditions

$$\tilde{T}(\mathring{r},\mathring{t} = 0) = \tilde{T}_i(\mathring{r}) \quad \text{and} \tag{A7a}$$

$$\tilde{T}(\mathring{r},\mathring{t})|_{\mathscr{S}} = \tilde{T}_1(\mathring{t}), \tag{A7b}$$

where $\mathscr{S}$ is the surface of the colloid (or a part of it) and T_1 is the temperature quench. In the following, we take $\tilde{T}_1$ to be time-independent. Equations (A4)–(A6) are turned into dimensionless ones by using the substitutions $\mathring{r} = rr_0$, $\mathring{t} = tt_0$, $\mathring{\psi}(\mathring{r},\mathring{t}) = \psi(\mathbf{r},t)\psi_0$, and $\mathring{\eta}(\mathring{r},\mathring{t}) = \eta(\mathbf{r},t)\eta_0$, where the quantities without $\circ$ are dimensionless and those with index 0 are the rescaling factors. This leads to the dimensionless CHC equation for an inhomogeneous temperature field, which is a solution of the HD equation:

$$\frac{\partial \psi(\mathbf{r},t)}{\partial t} = \nabla^2 \left(\frac{\tilde{T}(\mathbf{r},t)}{\tilde{T}_1}\psi(\mathbf{r},t) + \psi^3(\mathbf{r},t) - \nabla^2\psi(\mathbf{r},t) \right)$$
$$+ \eta(\mathbf{r},t) \tag{A8}$$

with

$$\frac{\partial \tilde{T}(\mathbf{r},t)}{\partial t} = \mathcal{D}\nabla^2\tilde{T}(\mathbf{r},t). \tag{A9}$$

$\mathcal{D}|\tilde{T}_1|$ is the so-called Lewis number [30], which is the ratio of the thermal diffusivity D_{th} and the interdiffusivity D_m of the solvent; we neglect the dependence of D_{th} and M on ψ. Although the bulk ordering field h_b does not enter Eq. (A9) explicitly, the dynamics depends on it implicitly via the conservation of the integral over the order parameter as a function of time. Upon rescaling, the Gaussian random noise obeys the relation $\langle \eta(\mathbf{r},t)\eta(\mathbf{r}',t')\rangle = -2\nu(\mathbf{r})\nabla^2\delta(\mathbf{r} - \mathbf{r}')\delta(t - t')$. The amplitude $\nu(\mathbf{r}) = [T(\mathbf{r})u/(T_c\tilde{T}_1^2)](|\tilde{T}_1|/C)^{d/2}$ is the strength of the dimensionless noise $\eta(\mathbf{r},t)$, which we take at $T(\mathbf{r}) = T_1$. The rescaling factors are given by

$$r_0 = \sqrt{C/|\tilde{T}_1|} = \sqrt{2}\xi_-(T_1), \tag{A10a}$$

$$t_0 = C\upsilon/\left(Mk_B T_c\tilde{T}_1^2\right) = 2\xi_-^2(T_1)/[D_m(T_c)|\tilde{T}_1|], \tag{A10b}$$

$$\psi_0 = \sqrt{|\tilde{T}_1|/u}, \tag{A10c}$$

$$\eta_0 = \sqrt{|\tilde{T}_1|/u}/\left[C\upsilon/\left(Mk_B T_c\tilde{T}_1^2\right)\right], \tag{A10d}$$

and

$$\mathcal{D} = D_{\text{th}}/(|\tilde{T}_1|D_m). \tag{A10e}$$

This amounts to expressing time in units of $(2\xi_-^2)/[D_m(T_c)|\tilde{T}_1|]$, where $D_m = M(k_B T_c/\upsilon)$ is the interdiffusion constant of the solvent at T_c and the OP in terms of $|\psi_b|$, which is the absolute value of the mean-field bulk OP at $T = T_1$; $\upsilon = a_0^d$, where a_0 is a microscopic length scale, e.g., the molecular size of the solvent molecules. Note that Eq. (A7) depends explicitly on $\tilde{T}_1$. This is so because we have chosen to express the physical quantities in dimensional units, which are taken at the temperature T_1. For example, the position vector $\mathbf{r}$ is expressed in units of the mean-field bulk correlation length $\sqrt{2}\xi_-$ at $T_1 < T_c$ and the OP in terms of $|\psi_b|$, which is the absolute value of the mean-field bulk OP at $T = T_1$. This choice of units is arbitrary, i.e., one could use

instead another temperature T_0. This would lead to an explicit dependence of the evolution equation for ψ [Eq. (A9)] on T_0. But the solution would not depend on it; after changing the units back into dimensional ones, the dependence on T_0 would drop out. This is not the case for the quench temperature T_1. The dependence on it is always present in the solution via the boundary condition [Eq. (A7b)]. In the case of a spatially homogeneous and time-independent temperature field, the coefficient multiplying the term $\propto \psi(\boldsymbol{r},t)$ in Eq. (A9) reduces to 1. The solutions of Eq. (A9) are averaged over multiple independent initial configurations, but they are not averaged over the noise $\eta(\boldsymbol{r},t)$.

Equation (A9) is complemented by the following boundary conditions (b.c.) on the surface $\mathscr{S}$ of the colloid:

$$\tilde{T}(\boldsymbol{r})|_{\mathscr{S}} = \tilde{T}_1, \tag{A11a}$$

$$\hat{\boldsymbol{n}} \cdot \nabla \tilde{T}(\boldsymbol{r})|_{\mathscr{S}} = 0. \tag{A11b}$$

Here, $\hat{\boldsymbol{n}}$ denotes the unit vector perpendicular to $\mathscr{S}$ pointing into the colloid. To take into account the generic preference of the colloidal surface for one of the two components of the binary mixture, we consider a surface energy contribution $\frac{1}{2}\mathring{\alpha}\int_{\mathscr{S}}\mathring{\psi}^2 dS - \mathring{h}_s\int_{\mathscr{S}}\mathring{\psi}\,dS$, which is added to $\mathring{\mathcal{F}}$ [19]. Here, $\mathring{\alpha}$ is a surface enhancement parameter and $\mathring{h}_s$ is a symmetry-breaking surface field. Upon the substitutions $\mathring{\alpha} = (C/|\tilde{T}_1|)^{-1/2}\alpha$ and $\mathring{h}_s = [(|\tilde{T}_1|/u)^{1/2}/(C/|\tilde{T}_1|)^{-1/2}]h_s$ this gives the dimensionless static, so-called Robin BC $[\hat{\boldsymbol{n}} \cdot \nabla\psi(\boldsymbol{r}) + \alpha\psi(\boldsymbol{r})]|_{\mathscr{S}} = h_s$ [19] with $\hat{\boldsymbol{n}}$ pointing into the colloid. The second necessary BC [20] corresponds to the requirement that there is no particle flux normal to the surface: $j_{\perp} = [-M\hat{\boldsymbol{n}} \cdot \nabla\mu(\boldsymbol{r},t) + \eta(\boldsymbol{r},t)]|_{\mathscr{S}} = [-M\hat{\boldsymbol{n}} \cdot \nabla\delta\mathcal{F}[\psi]/\delta\psi(\boldsymbol{r},t) + \eta(\boldsymbol{r},t)]|_{\mathscr{S}} = 0$ with the local chemical potential $\mu(\boldsymbol{r},t)$. For a homogeneous colloid, the *initial* configuration is prepared as follows: (i) Outside the colloid each lattice point of the simple-cubic simulation grid carries an OP value that is chosen randomly from a uniform random number distribution within the interval $[0,2\psi_0]$, such that the spatially averaged OP is ψ_0. (ii) All grid points, i.e., those for the binary liquid mixture outside the colloid as well as those for the inside of the colloid, receive a reduced temperature value $\tilde{T}_i = 1$ (above an upper critical temperature T_c). At $t = 0$, the values at the lattice points forming the surface of the colloid are quenched to $\tilde{T}_1 < 0$ (below an upper T_c). The ensuing temperature and order parameter profiles as a function of time are obtained by solving Eqs. (A9) and (A8) using the finite-element (FE) method. To implement the BC on a curved surface, a trilinear interpolation method [31] is used. All numerical results presented here are obtained for $\mathcal{D} = 50$ and for a numerical time step $dt = 0.001$ within the FE scheme.

APPENDIX B: PARAMETERS

The dimensionless parameters used in our numerical calculations can be expressed as ratios of certain dimensional quantities, which can be inferred from observables of a physical

realization of the system under consideration. The size of the simulation box and the radius of the colloid are $L/r_0 = 100$ and $R/r_0 = 10$, respectively, in the reduced units of the CHC theory. According to Eq. (A10a), this corresponds to $L = 141.4\xi_-$ and $R = 14.14\xi_-$ in dimensional units; ξ_- is the bulk correlation length of the binary liquid mixture at the quench temperature T_1 below T_c of demixing. These values can be related to the reduced temperature $\tau_1 = (T_1 - T_c)/T_c$ via the relation $\tilde{T}_1 = \mathcal{A}\tau_1$, where $\mathcal{A} = C/(\xi_0^+)^2$. Typically, for binary liquid mixtures the bulk correlation length amplitude is $\xi_0^+ \simeq 0.2$ nm [32,33]. The coefficient C is proportional to λ^2, where λ is the range of the correlations in that solvent [34] far away from the critical point, which we take to be about four times the size a_0 of the molecules. Typically, for water mixed with organic molecules one has $a_0 \simeq 3.4$ Å so that $C \simeq 1.85$ (nm)^2 and $\mathcal{A} \simeq 46.3$. We consider $\tilde{T}_1 = -1$ for the homogeneous colloid, which corresponds to $\tau_1 \simeq -0.02$. Using the relation $\xi_0^+/\xi_0^- \simeq 2$ [35] and the power law $\xi_- \simeq \xi_0^-|\tau_1|^{-\nu}$ with the critical exponent $\nu \simeq 0.63$ [35] of the three-dimensional Ising model, we obtain $\xi_-(\tau = -0.02) = 1.2$ nm, which yields the size of the simulation box and of the colloid as $L \simeq 170$ nm and $R \simeq 17$ nm, respectively. The time unit is $t_0 = 2\xi_-^2/[D_m(T_c)|\tilde{T}_1|]$, where $D_m(T = T_c)$ is the interdiffusion constant of the solvent at T_c. Note that this latter choice of temperature is by fiat because in the free-energy functional we take the reference free energy at T_c. Since we are not aware of any proper experimental analysis of the enhancement at criticality of and background contribution to the interdiffusion constant for any suitable binary liquid mixture, we replace $D_m(T_c)$ by the value of D_m at a very small reduced temperature $\tau_* = 10^{-6}$. For a water-lutidine mixture [32] this gives $D_m(\tau_* = 10^{-6}) \simeq 5 \times 10^{-14}$ m^2/s. Using the value of ξ_- as mentioned above, we obtain $t_0 \simeq 6 \times 10^{-5}$ s. Via the relation $D_{\text{th}} = \kappa/(\varrho C_P)$ the thermal diffusivity D_{th} can be expresses in terms of the mass density ϱ, the specific heat C_P, and the thermal conductivity κ of the fluid. For the 2,6-dimethylpyridine-water mixture near T_c, the values of ϱ and κ vary slightly with temperature whereas the variation of C_P is stronger [32,36,37]. Accordingly, we adopt the values of these quantities at 32 °C, i.e., $\varrho \simeq 990$ kg/m^3 and $\kappa \simeq 0.39$ W/(m K). The heat capacity C_P and the interdiffusivity D_m at $\tau_1 = 0.02$ (or for deeper quench $\tau_1 = 0.1$) as obtained from Ref. [32] are $7 J/(gK)$ $(8 J/(gK))$ and 4×10^{-11} m^2/s ($\approx 10^{-10}$ m^2/s), respectively, which renders $D_{\text{th}}(\tau = 0.02) \simeq 5.6 \times 10^{-8}$ m^2/s ($D_{\text{th}}(\tau = 0.1) \simeq 5 \times 10^{-8}$ m^2/s) so that with $|\tilde{T}_1| = 1$ ($|\tilde{T}_1| = 4.63$) and Eq. (10e), $\mathcal{D}(\tau = 0.02) = D_{\text{th}}(\tau = 0.02)/D_m(\tau = 0.02) \simeq 1.4 \times 10^3$ ($\mathcal{D}(\tau = 0.1) = D_{\text{th}}(\tau = 0.1)/D_m(\tau = 0.1) \simeq 10^2$) for $\tau = \tau_1$. The amplitude of the noise ν taken in our calculation is 10^{-4}–10^{-5}, which means that the strength of the dimensionless noise field can be estimated as $|\eta(\boldsymbol{r},t)| < \sqrt{\nu}$, i.e., it is one order of magnitude weaker than the dimensionless averaged order parameter $\psi_0 = 0.1$ used in our study. It is difficult to relate the surface parameters α and h_s used in our approach to physical observables. The small value of h_s corresponds to a weak preference for one component of the binary liquid mixture over the other.

[1] A. J. Bray, Adv. Phys. **43**, 357 (1994).

[2] K. Binder, in *Kinetics of Phase Transitions*, edited by S. Puri and V. Wadhawan (CRC, Boca Raton, FL, 2009), p. 62.

[3] S. K. Das, S. Puri, J. Horbach, and K. Binder, Phys. Rev. Lett. **96**, 016107 (2006).

[4] S. Puri, J. Phys.: Condens. Matter **17**, R101 (2005).

[5] H. Tanaka, J. Phys.: Condens. Matter **13**, 4637 (2001).

[6] J. Kumaki, T. Hashimoto, and S. Granick, Phys. Rev. Lett. **77**, 1990 (1996).

[7] Q. Tran-Cong and J. Okinaka, Polym. Eng. Sci. **39**, 365 (1999).

[8] P. K. Jaiswal, S. Puri, and K. Binder, Europhys. Lett. **103**, 66003 (2013).

[9] H. Jiang, N. Dou, G. Fan, Z. Yang, and X. Zhang, J. Chem. Phys. **139**, 124903 (2013).

[10] J. K. Platten and G. Chavepeyer, Physica A **213**, 110 (1995).

[11] G. Gonella, A. Lamura, and A. Piscittelli, J. Phys. A **41**, 105001 (2008).

[12] S. Hong and P. K. Chan, Modell. Simul. Mater. Sci. Eng. **18**, 025013 (2010).

[13] R. C. Ball and R. L. H. Essery, J. Phys.: Condens. Matter **2**, 10303 (1990).

[14] T. Araki and H. Tanaka, Europhys. Lett. **65**, 214 (2004).

[15] G. Volpe, I. Buttinoni, D. Vogt, H. J. Kammerer, and C. Bechinger, Soft Matter **7**, 8810 (2011).

[16] J. R. Gomez-Solano, A. Blokhuis, and C. Bechinger, Phys. Rev. Lett. **116**, 138301 (2016).

[17] A. Würger, Phys. Rev. Lett. **115**, 188304 (2015).

[18] S. Samin and R. van Roij, Phys. Rev. Lett. **115**, 188305 (2015).

[19] H. W. Diehl, Int. J. Mod. Phys. B **11**, 3503 (1997).

[20] H. W. Diehl and H. K. Janssen, Phys. Rev. A **45**, 7145 (1992).

[21] M. P. Allen and D. J. Tildesley, *Computer Simulations of Liquids* (Clarendon, Oxford, 1987).

[22] S. Roy and S. K. Das, Soft Matter **9**, 4178 (2013); J. Chem. Phys. **139**, 044911 (2013).

[23] B. P. Lee, J. F. Douglas, and S. C. Glotzer, Phys. Rev. E **60**, 5812 (1999).

[24] J.-P. Hansen and I. R. McDonald, *Theory of Simple Liquids* (Academic, London, 2008).

[25] R. Folk and G. Moser, J. Phys. A **39**, R207 (2006).

[26] T. Bickel, A. Majee, and A. Würger, Phys. Rev. E **88**, 012301 (2013).

[27] R. A. L. Jones, E. J. Kramer, M. H. Rafailovich, J. Sokolov, and S. A. Schwarz, Phys. Rev. Lett. **62**, 280 (1989).

[28] S. Puri and H. L. Frisch, J. Chem. Phys. **99**, 5560 (1993).

[29] R. Kurita, Sci. Rep. **7**, 6912 (2017).

[30] E. R. Cohen, T. Cvitas, J. G. Frey, B. Holmström, K. Kuchitsu, R. Marquardt, I. Mills, F. Pavese, M. Quack, J. Stohner, H. L. Strauss, M. Takami, and A. J. Thor, *Quantities, Units and Symbols in Physical Chemistry* (IUPAC & RSC, Cambridge, 2007).

[31] W. H. Press, S. A. Teukolsky, W. T. Vetterling, and B. P. Flannery, *Numerical Recipes in Fortran 77: The Art of Scientific Computing* (Cambridge University Press, Cambridge, 1986).

[32] S. Z. Mirzaev, R. Behrends, T. Heimburg, J. Haller, and U. Kaatze, J. Chem. Phys. **124**, 144517 (2006).

[33] E. Gulari, A. F. Collings, R. L. Schmidt, and C. J. Pings, J. Chem. Phys. **56**, 6169 (1972).

[34] N. Goldenfeld, *Lectures on Phase Transitions and Renormalization Group* (Addison-Wesley, Reading, MA, 1992).

[35] A. Pelissetto and E. Vicardi, Phys. Rep. **368**, 549 (2002).

[36] C. A. Gratonni, R. A. Dawe, C. Y. Seah, and J. D. Gray, J. Chem. Eng. Data **38**, 516 (1993).

[37] S. Pittois, G. P. Sinha, C. Glorieux, and J. Thoen, *Thermal Conductivity 27/ Thermal Expansion 15*, edited by H. Wang and W. Porter (DEStech, Lancaster, 2004).